JMEPEG (1999) 8:225-235

Texture Development and Hardening Characteristics of Steel Sheets under Plane-Strain Compression

P.A. Friedman, K.-C. Liao, J. Pan, and F. Barlat

(Submitted 4 March 1998; in revised form 2 December 1998)

Crystallographic texture development and hardening characteristics of a hot-rolled, low-carbon steel sheet due to cold rolling were investigated by idealizing the cold rolling process as plane-strain compression. The starting anisotropy of the test material was characterized by examination of the grain structure by optical microscopy and the preferred crystal orientation distribution by x-ray diffraction. Various heat treatments were used in an effort to remove the initial deformation texture resulting from hot rolling. The plastic anisotropy of the starting material was investigated with tensile tests on samples with the tensile axis parallel, 45°, and perpendicular to the rolling direction. The grain structure after plane-strain compression was studied by optical microscopy, and the new deformation texture was characterized by x-ray diffraction pole figures. These figures are compared with the theoretical pole figures produced from a Taylor-like polycrystal model based on a pencil-glide slip system. The uniaxial tensile stress-strain curve and the plane-strain, compressive stress-strain curve of the sheet were used to calibrate the material parameters in the model. The experimental pole figures were consistent with the findings in the theoretical study. The experimental and theoretical results suggest that the initial texture due to hot rolling was insignificant as compared with the texture induced by large strains under plane-strain compression.

Keywords cold rolling, plane-strain compression, steel, texture

1. Introduction

Conventional thermomechanical treatments of metals, such as hot and cold rolling, tend to produce microstructural anisotropy. This, in turn, can result in significant directionality of mechanical properties and hence change the optimal way to orient these materials in service conditions (Ref 1). Therefore, it is desirable to characterize the microstructural development within these materials resulting from thermomechanical treatments. This study focuses on the changes in microstructure, including grain structure and crystallographic texture, of a steel sheet under plane-strain compression and is one part of a comprehensive investigation of formability of body-centered cubic (bcc) steel sheets. One primary purpose of this study is to provide the necessary material parameters and validations for a companion study (Ref 2) on the texture development and plastic anisotropy of the bcc steel sheets.

A low-carbon, hot-rolled steel (AISI 1006) was selected as the test alloy for this investigation. Although this material had a nearly isotropic microstructure with respect to grain structure, it possessed a preferred crystal orientation, or rather a crystallographic texture. The initial microstructure of the hot-rolled steel sheet was characterized for both grain structure and crystal orientation. Various heat treatments followed by microstructural observation were applied to the test alloy in an effort to remove the initial texture. Because the material had been hot rolled and therefore was already recrystallized, it was predicted that a simple annealing heat treatment would not have an effect on the initial texture. Furthermore, it has been shown in literature (Ref 3, 4) that recrystallization textures are nearly identical to the as-rolled textures for bcc materials. However, it has been postulated by Walter et al. (Ref 5) and Weiner et al. (Ref 6) that deformation textures can be partially removed by inducing a phase change, such as austenitization. The effect of the initial anisotropy on the mechanical response of this alloy was investigated by performing tensile tests on samples with different orientations with respect to the rolling direction.

Rolling of sheet alloys causes lengthening and thinning of the sheet with very little width expansion. This width constraint is a result of deformation geometry in which the large ratio of width to indenting breadth creates a state of plane-strain compression. Therefore, it is possible to simulate rolling processes with plane-strain compression. To this end, plane-strain compression tests were performed both to analyze the effects of the constrained deformation on the microstructure and to quantify the hardening characteristics of the material during cold rolling. Specimens of various width-to-thickness ratios were studied to investigate the effect of specimen geometry on deformation. Optical microscopy was used to study the grain structure of the post formed material, and the development of crystallographic texture was examined with x-ray diffraction pole figures. These figures are pictorial representations of the orientation of certain planes within a material. They quantify the frequency that particular planes are in certain orientations with respect to the specimen geometry.

2. Materials

The hot-rolled, low-carbon steel, designated AISI 1006 (0.025C-0.12wt%Mn), in the form of a 203 by 305 by 5 mm sheet provided by Ford Motor Company was used for this

P.A. Friedman, Ford Research Laboratory, Dearborn, MI 48121; **K.-C. Liao** and **J. Pan,** Department of Mechanical Engineering and Applied Mechanics, University of Michigan, Ann Arbor, MI 48109; and **F. Barlat,** Alcoa Technical Center, Alcoa Center, PA 15069.

study. A blanchard grinder was used on the as-received material to produce samples of various thicknesses, ranging from 3.8 to 0.53 mm. The material was mechanically ground and polished and then etched with a 5% nital solution (5% nitric acid, 95% ethanol) in order to reveal the initial grain structure. Figures 1(a) and (b) show this microstructure in the L-T (plane containing the rolling and transverse directions) and L-S (plane containing the rolling and thickness directions) planes, respectively.

3. Experimental Procedures

Plane-strain compression tests were used to simulate both the hardening characteristics and the microstructural development during cold rolling of the material under study. It was desirable that the starting material have as near a random structure as possible with respect to both grain structure and crystal orientation. The initial microstructure was explored by examining the microstructure through optical and x-ray diffraction techniques. As shown in Fig. 1(a) and (b), it appears that the grain structure resulting from the thermomechanical treatment (i.e., hot rolling) was nearly equiaxed. The grain anisotropy ratio, defined as the average grain size in the rolling direction to the

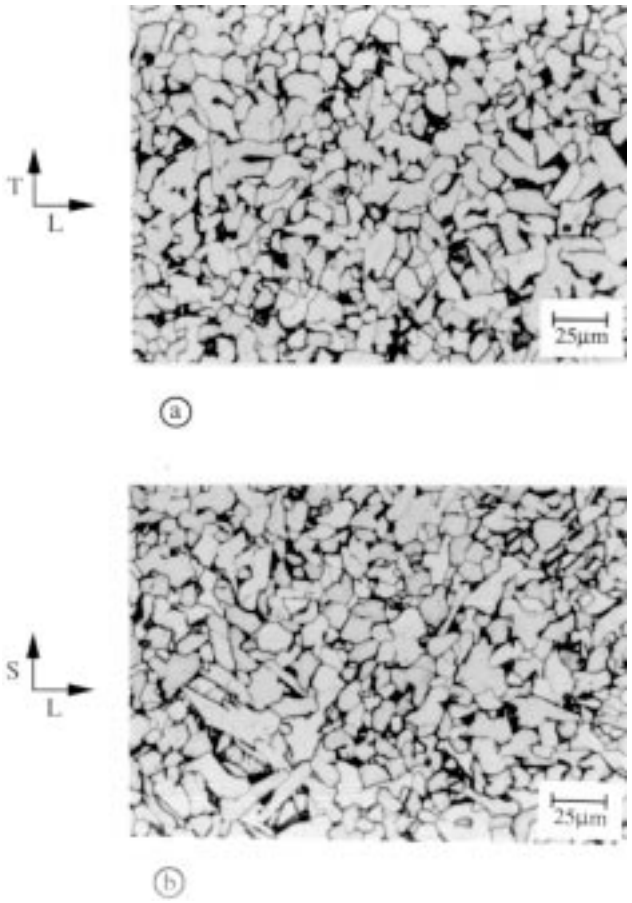

Fig. 1 Micrographs of the starting material depicting the grain structure in the (a) L-T plane (plane containing the rolling and transverse directions) and (b) L-S plane (plane containing the rolling and thickness directions)

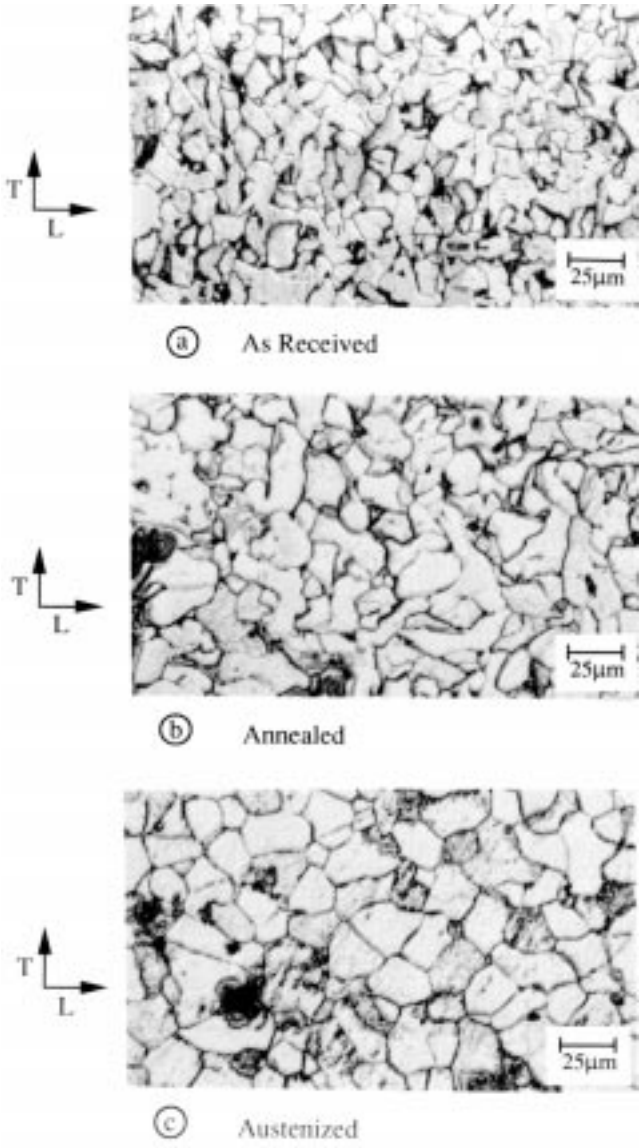

Fig. 2 Micrographs of the (a) as-received, (b) annealed, and (c) austenitized specimens depicting the grain structure in the L-T plane (plane containing the rolling and transverse directions)

Table 1 Heat treatments applied to test material

Type	Temperature, °C	Time, min	Atmosphere	Cooling	Comment
Annealing	550	65	Air	Air	Placed in preheated furnace
Austenitizing	950	15	Positive argon pressure	Furnace	Furnace ramped up to temperature in 90 min

average grain size in the thickness direction, was found to be approximately 1.15 for the as-received material.

Heat Treatments

Two different heat treatments were applied to the as-received material in an attempt to remove the rolled texture developed during thermomechanical processing. The first consisted of a simple recrystallization step followed by air cooling, while the other consisted of an austenitization step, which induced a phase change in the material from bcc to face-centered cubic (fcc), followed by a furnace cool. Table 1 lists these two heat treatments. The effects of these treatments on the microstructure were determined by x-ray diffraction analysis of the crystallographic orientation and through optical microscopy techniques discussed previously.

Figure 2 shows micrographs of material prior to and after heat treatments in the L-T orientation. It appears that the material experienced significant grain growth during these treatments. Grain sizes in the three principal directions (rolling, transverse, and thickness) were measured for each of the three different cases via the mean linear intercept method, plotted in Fig. 3. It appears that the grains grew proportionally in all three directions, and the slight degree of grain anisotropy in the as-received material was not affected by the heat treatments.

X-ray diffraction peak intensities were used to explore how the heat treatments affected the crystallographic orientation. Relative diffraction intensities were recorded over a wide range of angles (2 to 60°). Theoretical diffraction angles, listed in Table 2, were calculated based on the Bragg law (for example, see Ref 7), interatomic spacing of α-iron (2.866 Å), and the wavelength of copper Kα x-rays (1.542 Å). In Table 2, θ represents the diffraction angle. Because the diffraction angle is only a function of the x-ray wavelength, diffraction plane, and interatomic spacing, it was anticipated that the measured peaks for any one particular plane would occur at the same angle for all of the specimens. This is consistent with the data reported in this article. A sample output from the computer-controlled diffractometer is shown in Fig. 4(a), depicting diffracted intensity as a function of 2θ.

Table 2 Theoretical diffraction angles defined by the Bragg law

2θ, degrees	Plane
44.7	110
65.1	200
82.4	211
99.1	220

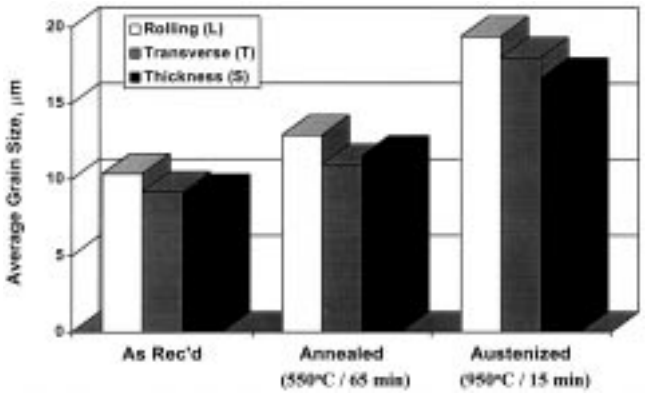

Fig. 3 Graphic representation of the degree of grain anisotropy in the as-received, annealed, and austenitized specimens. Grain size was measured by the mean linear intercept method.

The relative diffracted intensities from the (200), (211), and (220) planes, normalized with respect to the diffraction intensity from the (110) plane, are shown in Fig. 4(b). That is, the relative intensities for each specimen are percentages of the diffracted intensity from the (110) plane for that specimen. This representation of the data offers a convenient method of quantifying the degree of preferred orientation in the material. The relatively low peaks from the as-received specimen indicate that some degree of texture was formed in the material during thermomechanical treatment. As predicted, the annealing heat treatment had very little effect on the initial texture. This is shown in Fig. 4(b), where only a small increase in diffraction peaks from the annealed specimen was detected as compared with that of the as-received material. Contrary to this, the diffraction peaks were significantly greater for the austenitized specimen, possibly indicating that this heat treatment may have modified the initial texture.

It has been suggested that repeated austenitizations followed by cooling can further reduce this deformation texture. However, this temperature cycling, because of slow furnace cooling, would be at the expense of grain growth and may pres-

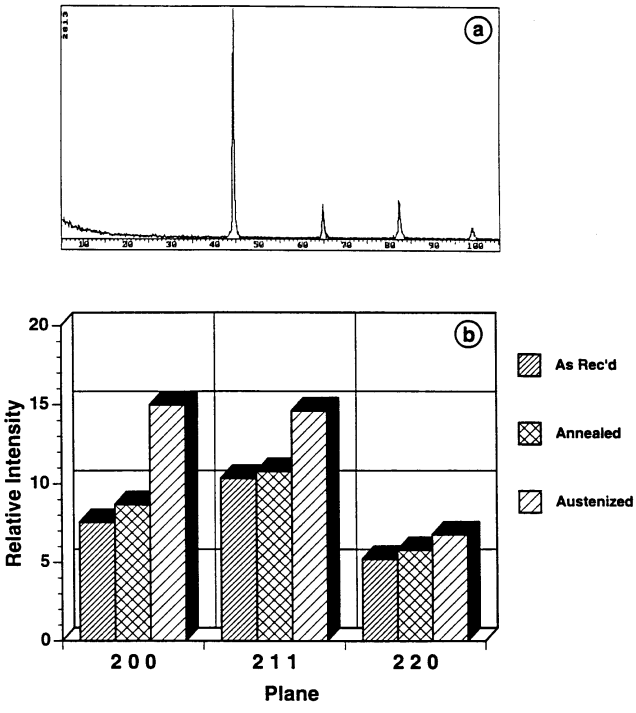

Fig. 4 (a) Example output of intensity versus 2θ from the computer-controlled diffractometer used in this study. (b) The relative intensity peaks with respect to the (110) plane from the as-received, annealed, and austenitized specimens

ent problems with the development of x-ray diffraction pole figures. In view of this, the as-received material was chosen for the study, and the initially preferred orientation was quantified with pole figures. It was found that this initial texture was of little consequence in the development of the deformation texture resulting from plane-strain compression at large compressive strains.

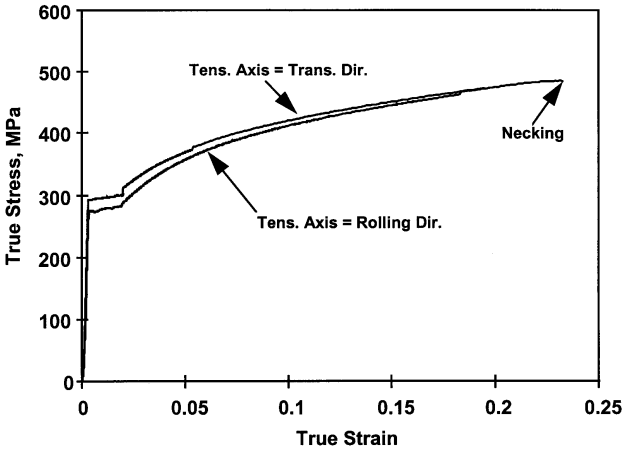

Fig. 5 The converted true stress versus true strain plots from tensile tests conducted on specimens with the tensile axis both parallel and perpendicular to the rolling direction

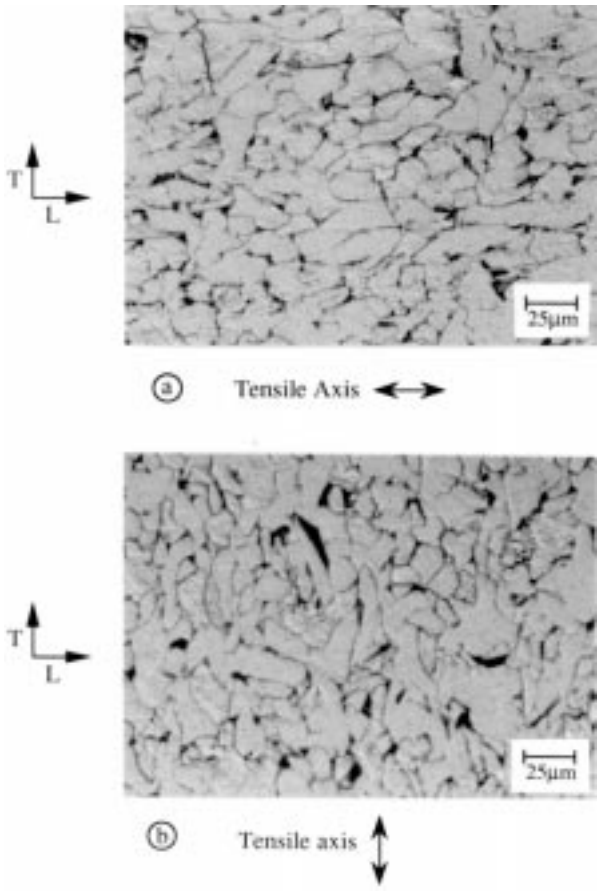

Fig. 6 Micrographs depicting the grain structure in the L-T plane (plane containing the rolling and transverse directions) after deformation in tensile specimens oriented with the tensile axis (a) parallel and (b) perpendicular to the rolling direction

Tensile Tests

The effect of anisotropy on the mechanical response of the as-received material was investigated by performing tensile tests on specimens with the tensile axis oriented parallel, 45°, and perpendicular to the rolling direction. Tests were conducted in a computer-controlled 4505 Instron machine (Instron Corporation, Canton, MA). Tensile specimens were prepared from ground and polished sheets via a milling apparatus specifically designed to prepare tensile specimens from sheet materials. Specimens were milled to a gage length of approximately 100 mm, a width of 12 mm, and a sheet thickness of 2.7 mm. The Instron was driven at a constant crosshead speed of 0.6 mm/min, and specimens were pulled until maximum load was attained. A 12.7 mm extensometer was attached to the middle section of the gage length to monitor nominal strain throughout the test.

The resulting nominal stress versus nominal strain curves for tests run on longitudinal (tensile axis parallel to the rolling direction) and transverse (tensile axis perpendicular to the rolling direction) specimens, respectively, were converted to true stress versus true strain curves with the assumptions of pure uniaxial deformation and uniform straining within the gage region. Figure 5 shows the true stress versus true strain curves as well as the point at which necking begins to occur. The difference in the yield stresses between the transverse and longitudinal specimens, depicted in Fig. 5, is further evidence of an initial anisotropy. However, the effects of the initial anisotropy tend to disappear with continued straining as seen from the similar hardening characteristics of the two samples.

Another method of quantifying plastic anisotropy is through the strain ratio, R, defined as the ratio of width strain to thickness strain during a tensile test. For an isotropic material in uniaxial tension, the value of R is 1. A very large R value (i.e., 3 to 7) suggests a large resistance to thinning in the material (Ref 1). Because the strain ratio tends to vary with respect to the direction of the tensile axis, an average value of strain ratio, R, is often reported. According to Hosford and Caddell (Ref 8) this value can be calculated as:

$$\overline{R} = \frac{R_0 + 2R_{45} + R_{90}}{4} \qquad \text{(Eq 1)}$$

where R_0, R_{45}, and R_{90} are the strain ratios from specimens with the tensile axis parallel, 45°, and perpendicular to the rolling direction, respectively. Strains were measured from the tensile tests in the width and thickness directions with a point mi-

Table 3 Strain ratio values determined from tensile tests

Direction	R	ε_w	ε_t
R_0	1.09	0.112	0.102
R_{45}	1.01	0.131	0.130
R_{90}	1.16	0.119	0.102
$\overline{R}$	1.07	…	…

crometer and listed with the corresponding strain ratio values in Table 3. It appears from these strain ratio values that the material did not display any significant degree of anisotropy after a tensile strain of approximately 0.2 was reached. However, it is possible that the material had a significant amount of anisotropy at the initiation of plastic straining. With further straining this anisotropy disappeared, and the material emulated that of a nearly isotropic material.

The microstructures of the deformed tensile specimens were examined to gain information on the effect of the deformation on the grain structure. Figure 6 shows micrographs of these specimens in the L-T orientation. It appears as if the deformation resulted in a large degree of grain elongation, producing an elongated grain structure in the direction of the tensile axis. Further, it does not seem as if the slight degree of initial grain anisotropy, resulting from the hot rolling, had any significant effect on the formation of this new grain structure.

Plane-Strain Compression

Plane-strain compression tests were performed to simulate the rolling process and investigate the subsequent strain hardening behavior and microstructural development in this alloy. The miniature press used for these experiments, shown in Fig. 7, was placed in an Instron 4505 machine, which was used for control of deformation and accurate measure of loads. Figure 8 is a pictorial representation of a plane-strain compression specimen within the press depicting the pertinent specimen dimensions. The criteria on these dimensions for plane-strain compression, as defined by Caddell (Ref 9), are:

$$w/b > 6 \qquad \text{(Eq 2)}$$

$$2 < b/t < 4 \qquad \text{(Eq 3)}$$

where w, b, and t are defined in Fig. 8. A specimen compression area of 1.5 by 12 mm (i.e., b = 1.5 mm and w = 12 mm), which adheres to the constraint of Eq 2, was chosen for all the tests. The as-received plate was ground to four different thicknesses in order to investigate the second criterion, Eq 3. Table 4 lists these initial thicknesses as well as the associated b to t ratios. The two thinnest specimens (i.e., largest b to t ratios) satisfied the criterion for plane-strain compression, Eq 3, while the other two specimens were thicker than the criterion allowed.

Tests were conducted by compressing specimens to different amounts of deformation and recording the peak loads from the Instron. Layers of Teflon coated with mineral oil were placed between the specimen and press surfaces to minimize the frictional effects associated with compression tests. Strains were determined by accurate measurement of final thicknesses with a point micrometer after compression. Using this method rather than crosshead displacement of the Instron eliminated problems associated with system compliance. Six compression strains were made on each of the different specimens.

Table 4 Specimen dimensions for plane-strain compression

Thickness, mm	*b/t*
2.71	0.55
1.49	1.00
0.74	2.02
0.53	2.85

The stress data were adjusted for friction from a simple sliding friction model developed by Hosford (Ref 1) that relates the indent pressure to the actual compressive stress through the specimen dimensions and the coefficient of friction. This can be expressed as:

$$\sigma = \frac{\mu b}{t} \frac{1}{\left[\exp\left(\frac{-\mu b}{t}\right) - 1\right]} \sigma_{avg} \qquad \text{(Eq 4)}$$

where σ is the corrected flow stress, μ is the coefficient of friction, and σ_{avg} is the average contact stress, as recorded by the Instron. The coefficient of friction was assumed to be 0.065, which lies between 0.05 and 0.08, values typical for this type of lubrication. The stress data were transformed to those of the effective stress (based on the von Mises criterion) with:

Fig. 7 Photograph of the miniature press used for the plane-strain compression tests

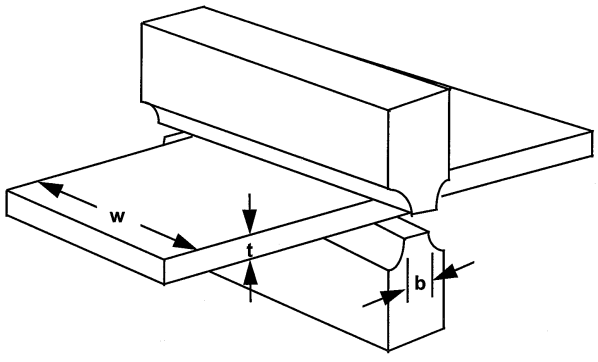

Fig. 8 Pictorial representation of the press and specimen (including specimen dimensions) used for plane-strain compression tests

$$\bar{\sigma} = \frac{1}{\sqrt{2}}[(\sigma_1 - \sigma_2)^2 + (\sigma_2 - \sigma_3)^2 + (\sigma_3 - \sigma_1)^2]^{1/2} \quad \text{(Eq 5)}$$

where $\bar{\sigma}$ is the effective stress, and σ_1, σ_2, and σ_3 are the principal stresses in the thickness, width, and simulated rolling directions, respectively. The effective stress definition is simplified with the assumption of plane-strain compression with the strain in direction 2 and the stress in direction 3 taken as zero. Equation 5 simplifies to:

$$\bar{\sigma} = \frac{\sqrt{3}}{2}\sigma_1 \quad \text{(Eq 6)}$$

Similarly, the effective strain based on the same assumptions is defined as:

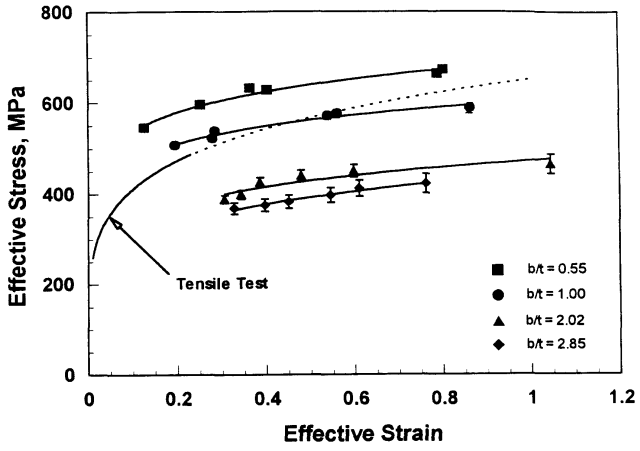

Fig. 9 Effective stress versus effective strain plots for plane-strain compression tests corrected for friction performed on specimens with a range of breadth to thickness ratios (*b*/*t*). The hardening behavior from the tensile test, extrapolated from the power-law relation to a strain of 1.0, is also shown for comparison.

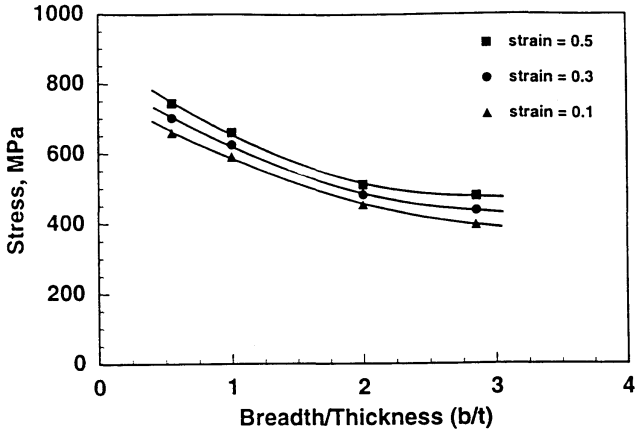

Fig. 10 Stress values of specimens deformed in plane-strain compression to equal strain levels plotted as functions of breadth to thickness ratio (*b*/*t*)

$$d\bar{\varepsilon} = \frac{2}{\sqrt{3}}d\varepsilon_1 \quad \text{(Eq 7)}$$

where $d\bar{\varepsilon}$ and $d\varepsilon_1$ are increments of the effective strain and the strain in direction 1, respectively.

The effective stress-effective strain data, corrected for friction with Eq 4 and a coefficient of friction value of 0.065, are plotted in Fig. 9. Error bars depict the spread of data resulting from coefficient of friction values of 0.05 to 0.08. The hardening behavior from the tensile test, extrapolated from the power-law relation to a strain of 1.0, is also shown in Fig. 9 for comparison. It is evident from this data that as the *b* to *t* ratio increases from a relatively thick specimen to a specimen more consistent with plane-strain compression, there is a significant decrease in the effective stress. Data for each specimen geometry were fit with the simple power-law hardening equation:

$$\bar{\sigma} = k\bar{\varepsilon}^n \quad \text{(Eq 8)}$$

where $\bar{\sigma}$ and $\bar{\varepsilon}$ are the effective stress and strain, respectively. The values of the constants *k* and *n* are listed in Table 5.

It appears that the decrease in the effective stress, with changes in specimen thickness, begins to decline for thinner specimens. This is shown in Fig. 10 where this same stress data is plotted as a function of the initial *b* to *t* ratio for several levels of strain. It is possible that the effective stresses are asymptotically approaching a fixed value with further decreases in specimen thickness. Furthermore, it appears in Table 5 and Fig. 9 that the hardening rate is greatest for the tensile test, reaching stresses in excess of the thinner two specimens, which meet the plane-strain compression criterion in Eq 3. However, the hardening curve for the tensile test has been extrapolated from the measured stress-strain data and therefore may not be completely indicative of the true hardening characteristics of the material under uniaxial tensile conditions.

The effect of rolling processes on the grain structure was examined by revealing the microstructure after plane-strain compression. Figures 11(a) and (b) show the grain structures of the specimen before and after plane-strain compression, respectively. In the figure, *t* indicates the thickness direction and *b* indicates the equivalent rolling direction. Figure 11(b) shows the extremely elongated grain structure in the equivalent rolling direction (parallel to the *b* dimension) in the compressed sample. It also appears as though the small degree of grain anisotropy found in the initial material (Fig. 11a) was negligible with respect to this new deformed grain structure Fig. 11(b).

Table 5 Power-law hardening constants

b/t	*k*, MPa	*n*
0.55	689.2	0.108
1.00	604.6	0.105
2.02	473.2	0.144
2.85	443.0	0.178
Tensile test	653.1	0.201

Pole Figures

Texture development in this material during plane-strain compression was quantified with x-ray diffraction pole figures. Larger plane-strain compression samples (w = 101.6 mm, b = 12.7 mm, and t = 3.3 mm), which adhered to the criteria of Eq 2 and 3, were machined to provide test specimens that satisfied the size requirement of the x-ray diffraction equipment. These specimens were compressed to two different levels of strain in a 250 ton Instron press equipped with a similar press, as shown in Fig. 7. As in earlier tests, Teflon with mineral oil was used as a lubricant between the press and the specimen surfaces. The crosshead was moved at a constant velocity of 2.5×10^{-2} mm/s, and the thickness strains, as measured by a point micrometer, of 0.34 and 0.79 were achieved.

Small sections of the deformed material (15 by 10 mm) were cut from the tested samples and prepared for x-ray diffraction. The surfaces of compressed material typically contain remnants of deformation caused by the contact, and because back reflection x-ray analysis reaches a penetration depth of only 10 to 15 μm, it was essential that surface material be removed prior to x-ray analysis. To this end, material was alternately mechanically ground and etched with a 5% nital solution (5% nitric acid, 95% ethanol) until a near optically perfect surface was attained.

Pole figures of the (110) and (200) planes, whose 2θ values are listed in Table 2, were produced for the untested material as well as for the two deformed samples. Specimens were oriented so that the simulated rolling direction was oriented at the top of the pole figure, ($\phi = \delta = 0°$), as depicted in Fig. 12(a) and (b). X-ray diffraction data were normalized, corrected for background scatter, and recalculated to produce the pole figures. Figures 13(a) and 14(a) show the resulting pole figures for the material prior to deformation in the (110) and (200) planes, respectively. The contour lines define lines of constant intensity. As shown in Fig. 13(a), the orientation of the (110) planes in the untested material seem to be fairly evenly distributed, displaying only a slight degree of preferred orientation. The effect of the deformation in terms of the (110) planes is shown in Fig. 13(b) and (c) for strains of 0.34 and 0.79, respectively. It appears from these figures that a considerable amount of grain reorientation occurred, and a large degree of texture formed. This is most evident in the absence of any (110) planes in the center of the pole figure ($\phi = 90°$). The majority of the grains rotated such that the (110) planes were parallel to the transverse direction, displaying intensities at both the very edge of the figure (δ

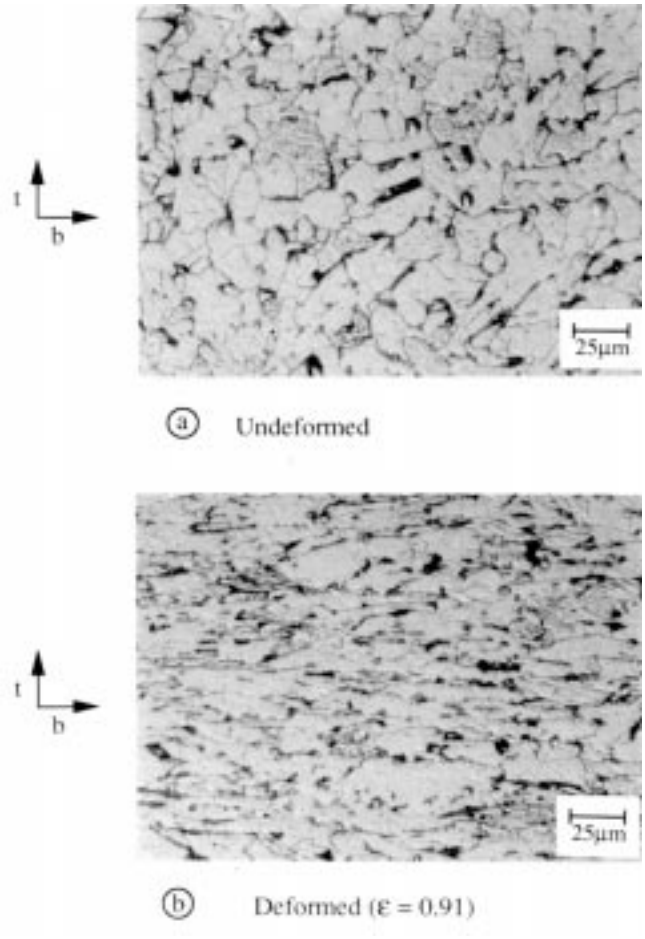

Fig. 11 Micrographs depicting the grain structure in the b/t orientation for a plane-strain compression specimen (a) before and (b) after deformation to the thickness strain of 0.91

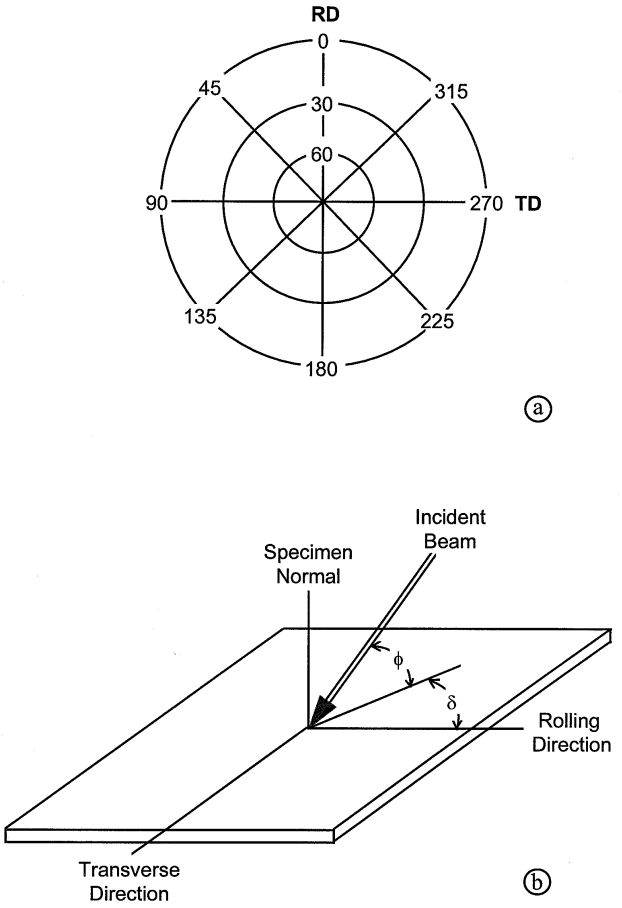

Fig. 12 (a) Sample pole figure depicting angles as well as the rolling (RD) and transverse (TD) directions. (b) Pictorial representation of the sample geometry and the angles δ and ϕ relative to the incident beam

= 0°, ϕ = 0°; δ = 180°, ϕ = 0°) and at approximately 30° off from the sheet normal (δ = 0°, ϕ = 60°; δ = 180°, ϕ = 60°). In other words, the concentrations are at a 30° angle with the sheet in the rolling direction and perpendicular to the sheet in the rolling direction.

The (200) pole figure of the untested material also shows a fairly even distribution of orientations with a possible concentration at the center of the figure (ϕ = 90°). The pole figures of the deformed specimens, Fig. 14(b) and (c), show a slightly more complicated orientation of planes than (110). The major concentration of (200) planes seems to be in the center of the figure with lesser concentrations tilted slightly toward the transverse direction (δ = 90°, ϕ = 45 to 90°; δ = 270°, ϕ = 45 to 90°). A second concentration of planes was also detected approximately 60° off from the sheet normal in the rolling direction extending across the top of the figure (δ = 60 to –60°, ϕ = 30°) and (δ = 120 to 240°, ϕ = 30°). Finally, there seems to be a concentration of (200) planes perpendicular to the sheet and parallel to the rolling direction (δ = 90°, ϕ = 0°) and (δ = 270°, ϕ = 0°).

The deformation textures found here are typical of many bcc materials that have been cold rolled (Ref 10-12). Considerable simulation work has been done predicting deformation textures. As a comparison to this work, simulated pole figures de-

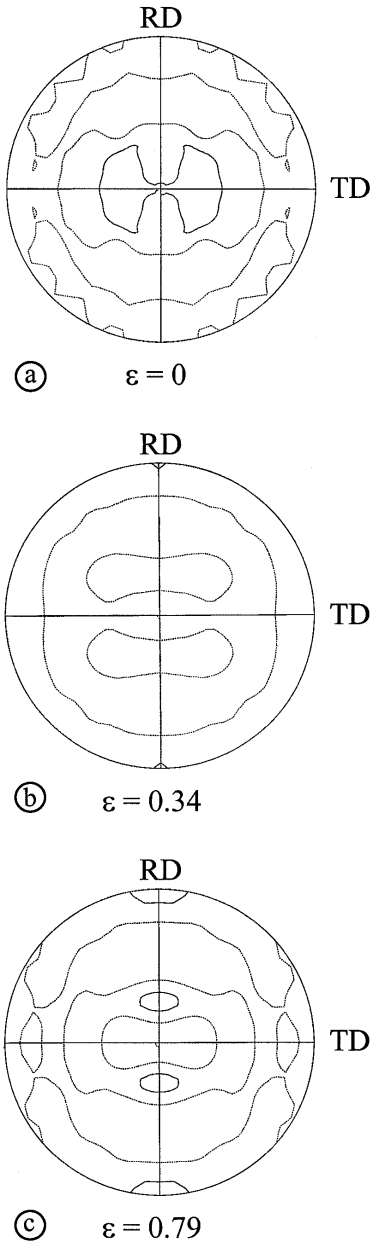

Fig. 13 (110) pole figures of the (a) material before compression, (b) material compressed to a strain of 0.34, and (c) material compressed to a strain of 0.79. Strain measurements are negative thickness strain.

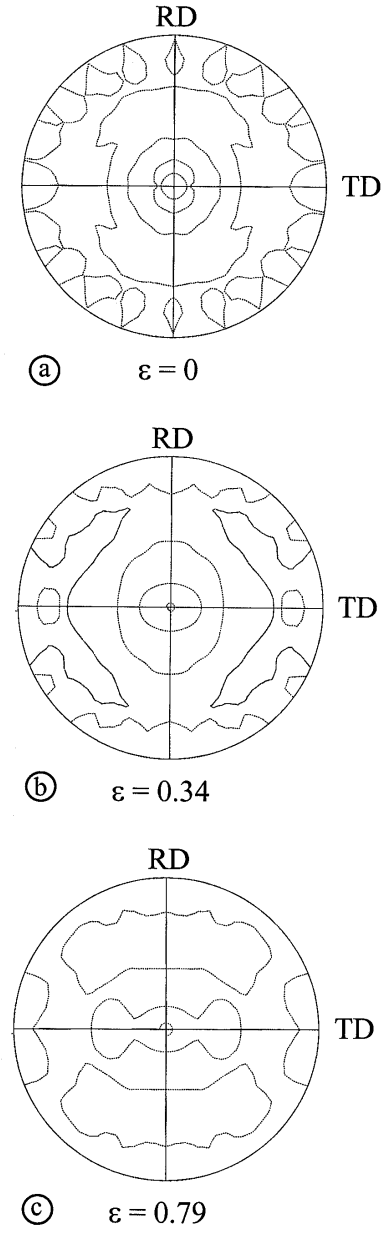

Fig. 14 (200) pole figures of the (a) material before compression, (b) material compressed to a strain of 0.34, and (c) material compressed to a strain of 0.79. Strain measurements are negative thickness strain.

veloped by Liao et al. (Ref 2) of a low-carbon steel deformed in plane-strain compression are shown in Fig. 15 and 16. These pole figures were developed at the same thickness strains of 0.34 and 0.79 for fair comparison with the experimental results (Fig. 13 and 14). Simulations were based on a Taylor-like model developed by Asaro and Needleman (Ref 13) and the <111> pencil glide slip system. It appears that the concentration patterns of the simulated pole figures show good agreement with the experimentally determined pole figures. Note that for a material with a completely random crystallographic orientation, the pole figure may appear to have a slight concentration in the center of the figure (Fig. 15 and 16) due to the nature of pole figures in general.

4. Discussion

To study microstructural development resulting from deformation processes, it is necessary that the initial microstructure be fully characterized. Further, it is beneficial to start with an isotropic material in order to quantify the development of a preferred texture resulting from deformation processes. To this

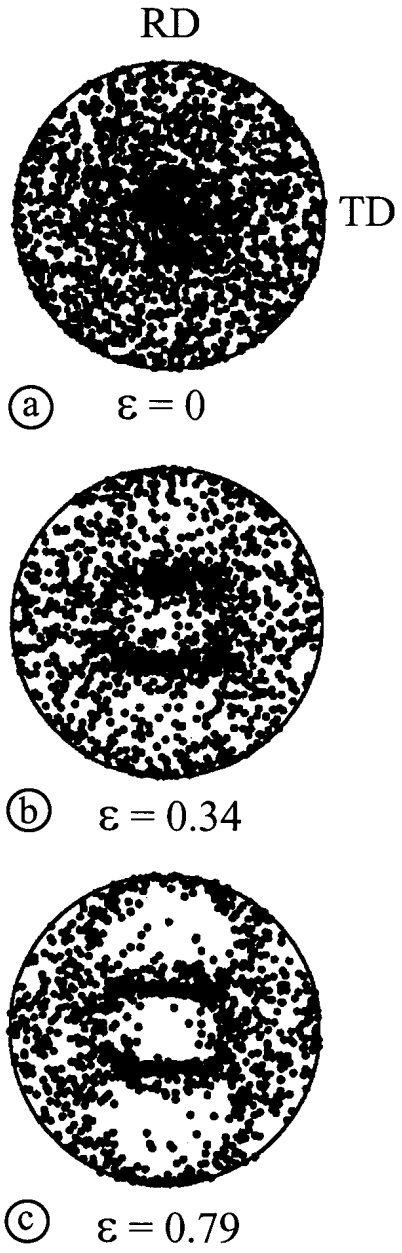

Fig. 15 (110) pole figures from simulations of plane-strain compression. Simulations were based on the Taylor-like model of Asaro and Needleman (Ref 13) and taken from Liao et al. (Ref 2). Strain measurements are negative thickness strain.

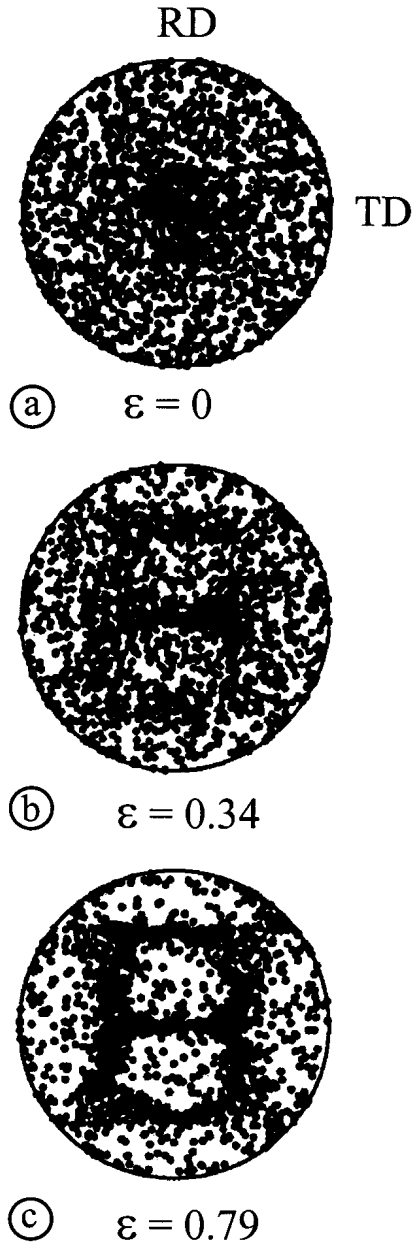

Fig. 16 (200) pole figures from simulations of plane-strain compression. Simulations were based on the Taylor-like model of Asaro and Needleman (Ref 13) and taken from Liao et al. (Ref 2). Strain measurements are negative thickness strain.

end, the initial material in this study was characterized with x-ray diffraction and optical microscopy techniques. The microstructure of the as-received sheet, shown in Fig. 1, displays a nearly equiaxed grain structure. This is a result of recovery processes at the relatively high temperatures during hot rolling of the sheet. Although the starting material was found to be nearly isotropic with respect to grain structure, it did not indicate an absence of a crystallographic texture. In fact, it is quite possible that materials after thermomechanical treatment have completely equiaxed grain structures while still displaying some texture, as was the case in this study.

Two different heat treatments, listed in Table 1, were performed in an attempt to remove this deformation texture. Because the starting material was already recrystallized, the annealing heat treatment had little effect on the texture while causing significant grain growth. This is shown in Fig. 4(b), where x-ray diffraction analysis after annealing is compared with the initial microstructure, and Fig. 2(b), where the grain structure of these specimens is shown. Inducing a phase change, by way of austenitization, was also attempted in an effort to remove this initial texture. This process, which also caused significant grain growth (Fig. 2c), did seem to have an effect on the preferred orientation. This is shown in Fig. 4(b), where the relative diffracted intensities from the (200), (211), and (220) planes, normalized with respect to the (110) plane, are greater for the austenitized specimen as compared with the as-received or annealed specimens. While it has been postulated that repeated austenitizations may further aid in removing the initial texture, it would have been at the expense of significant grain growth, which may have resulted in inaccurate x-ray diffraction pole figures.

To determine if this initial texture would present problems in this study, an analysis of the anisotropy with respect to the mechanical response of this material was performed. This was accomplished by performing tensile tests on specimens with the tensile axis parallel, 45°, and perpendicular to the rolling direction. While the yield stress was found to be slightly higher for the transverse specimen (Fig. 5), both specimens seemed to experience similar hardening behavior with continued straining. As shown in Fig. 6, the small degree of grain anisotropy in this material seems insignificant as compared with the extensive grain elongation in the direction of the tensile axis resulting from the deformation. This dominant new grain anisotropy developed during deformation may explain the similar hardening behavior between these two tests. In the initial stage of deformation, the starting anisotropy had a noticeable effect on the mechanical response of the material. This is seen in the different measured yield stresses for the two samples. With continued straining, the effects of the initial microstructure disappeared, and the grains in both tests elongated in the direction of the tensile axis. The early effects of the starting anisotropy were drowned out by the new dominant deformation grain structure. Therefore, with accumulated strain ($\varepsilon \sim 0.2$), the effects of the initial texture disappeared, and the hardening behavior of the two specimens converged.

To simulate the cold rolling process, plane-strain compression tests were performed on the steel sheets. Specimens of varying thicknesses were used in this study to analyze the effect of specimen breadth to thickness ratio (i.e. b/t) on strain hardening behavior. As this ratio increased (i.e., thinner specimens), there was a significant decrease in flow stress (Fig. 9). Further, it appears that these decreases in flow stress tapered off and may have asymptotically approached limiting stress values with increasing b to t ratios (Fig. 10). For specimens with lower b to t ratios, the flow stresses appear higher, possibly due to high compressive stresses developed similar to those under a flat punch on a semi-infinite solid. Note that the well-known Prandtl (Ref 14) solution for a flat punch on a semi-infinite, perfectly plastic solid under plane-strain conditions gives a plane-strain compression yield stress about three times the uniaxial yield stress as compared with the typical plane-strain compressive yield stress of 1.15 times the uniaxial yield stress (von Mises yield criterion). Further tests on a wider range of specimen geometries are needed to investigate this phenomenon. Comparison of these results, corrected for friction and transformed to von Mises effective stress and effective strain, indicate that the material experiences a slightly reduced hardening rate during plane-strain compression as compared with the extrapolated uniaxial tensile stress-strain relation (Fig. 9).

The effect of plane-strain compression on the microstructure was examined by optical microscopy. It appears from the micrographs shown in Fig. 11 that the grains experienced a large degree of stretching in the simulated rolling direction (i.e., direction parallel to the b dimension). This observation leads to the conclusion that the initial grain anisotropy had very little effect on the deformation and can be considered insignificant.

The x-ray diffraction pole figures (Fig. 13 and 14) showed that the initial material contained only a slight degree of preferred texture and that, with deformation, a particular texture was formed. The (110) plane in the starting material was nearly randomly distributed throughout the material with the possibility of a slight concentration of planes found 60° from the sheet surface in the transverse direction. With deformation, these planes switched orientation and displayed a tendency to tilt toward the rolling direction (Fig. 13b and c). Contrary to this behavior was that of the (200) plane. Initially this plane showed a dominant concentration of planes oriented parallel to the specimen surface with a slight preference in orientation at an angle between the specimen normal and the rolling direction. Pole figures of the deformed specimens show that, with straining, the (200) planes concentrate in several different orientations (Fig. 14b and c).

The significant changes in texture due to plane-strain compression and hence cold rolling can present large directional effects on the mechanical behavior of these materials. It is therefore desirable that these effects be quantified and understood so these materials can be used in the most efficient manner possible. Further work deciphering the effects of this deformation texture on the mechanical properties is needed to maximize the usefulness of these materials.

5. Summary and Conclusions

A low-carbon, hot-rolled steel sheet was deformed in plane-strain compression in order to investigate the mechanical be-

havior and subsequent microstructural development that occurs during cold rolling. The conclusions are:

- Annealing hot-rolled, low-carbon steels does not significantly change the texture resulting from thermomechanical treatments. However, inducing a phase change by austenitizing the material aids in removing the initial texture at the expense of significant grain growth.
- The preferred orientation formed during hot rolling results in a slight degree of anisotropy with respect to the mechanical properties. However with continued straining, this effect is drowned out as a new grain structure resulting from the tensile deformation becomes more dominant.
- This material experiences a significant degree of strain hardening during cold rolling, as determined by plane-strain compression tests. The post-yield behavior seems to be consistent with a power-law hardening model. However, the hardening rate in plane-strain compression appears to be significantly less than that of the extrapolated uniaxial tensile stress-strain relation.
- The specimen breadth-to-thickness ratio (b/t) in plane-strain compression has a profound effect on the flow stress in this alloy. Decreases in specimen thickness result in lower flow stresses. Further, these flow stresses may converge to certain limiting values with continued decreases in specimen thickness.
- The microstructure after plane-strain compression contains extremely elongated grains in the breadth direction, depicting a similar structure to that of cold-rolled sheet alloys.
- X-ray diffraction pole figures showed that the initial material contained only a slight degree of texture and that this texture was completely drowned out with the formation of a new texture resulting from the plane-strain compression.

Acknowledgments

The authors acknowledge the support for this work by the National Science Foundation under grant number DDM-9102424 and the University Research Program of Ford Motor Company. The assistance of J. Wu of Ford Motor Company to this research is greatly appreciated. Helpful discussions with Professor W.F. Hosford of the University of Michigan were also appreciated. Thanks are also given to E. Llewellyn (Alcoa Technical Center) for pole figure measurements.

References

1. W.F. Hosford, *The Mechanics of Crystals and Textured Polycrystals*, Oxford University Press, 1993
2. K.-C. Liao, P.A. Friedman, J. Pan, and S.C. Tang, Texture Development and Plastic Anisotropy of bcc Strain Hardening Sheet Metals, *Int. J. Solids Struct.*, Vol 35, 1998, p 5205-5236
3. J.L. Walter and C.G. Dunn, Tertiary Recrystallization in Silicon Iron, *Met. Soc. AIME*, Vol 218, 1960, p 366-367
4. W.C. Leslie, Control of Annealing Texture by Precipitation in Cold-Rolled Iron, *Met. Soc. AIME*, Vol 221, 1961, p 752-758
5. J.L. Walter, W.R. Hibbard, H.C. Fielder, H.E. Grenoble, R.H. Pry, and P.G. Frischmann, Magnetic Properties of Cube Textured Silicon-Iron Magnetic Sheet, *J. Appl. Phys.*, Vol 29, 1958, p 363-365
6. G. Weiner, P.A. Albert, R.H. Trapp, and M.F. Littmann, Cube Texture in Body Centered Magnetic Alloys, *J. Appl. Phys.*, Vol 29, 1958, p 366-367
7. B.D. Cullity, *Elements of X-Ray Diffraction*, 2nd ed., Addison-Wesley, Reading, Massachusetts, 1978
8. W.F. Hosford and R.M. Caddell, 2nd ed., Prentice-Hall, Englewood Cliffs, New Jersey, 1993
9. R.M. Caddell, *Deformation and Fracture of Solids*, Prentice-Hall, Englewood Cliffs, New Jersey, 1980
10. A. Segmüller and G. Wassermann, Walzteturen von Molybdän and Tantal, *Freiberger Forschungshefte*, Vol B38, 1960, p 38-44 (in German)
11. P. Parniere, Recrystallization Texture of Low Carbon Steel Sheets, *Fifth Int. Conf. on Textures of Materials*, Springer-Verlag, 1981, p 181-194
12. H. Inagaki, Transformation Textures in Control-Rolled High Tensile Strength Steel, *Sixth Int Conf. on Textures of Materials*, Iron and Steel Institute of Japan, 1978, p 157-166
13. R.J. Asaro and A. Needleman, Texture Development and Strain Hardening in Rate Dependent Polycrystals, *Acta Metall.*, Vol 33, 1985, p 923-953
14. L. Prandtl, Über die Härte Plastischer Koerper, *Goettinger Nachr. Math. Phys.* Kl., 1920, p 74-85 (in German)